Electronic Supporting Information for

Unravelling Photoisomerization Dynamics in a Metastable-State Photoacid

*Ying-Zhong Ma,[1] * Uvinduni I. Premadasa,[1] Vyacheslav S. Bryantsev,[1] Audrey R. Miles,[1,2] Ilia N. Ivanov,[3] Adnan Elgattar,[4] Yi Liao,[4] Benjamin Doughty[1]*

[1]Chemical Sciences Division, Oak Ridge National Laboratory, P.O. Box 2008, Oak Ridge, TN 37831

[2]Department of Chemistry and Biochemistry, University of Notre Dame, Notre Dame, IN 46556

[3]Center for Nanophase Materials Sciences, Oak Ridge National Laboratory, Oak Ridge, TN 37831

[4]Department of Biomedical and Chemical Engineering, Florida Institute of Technology, Melbourne, FL 32901

*Corresponding author: may1@ornl.gov

This PDF file includes:

Experimental and Computational Methods

Supporting Experimental Results: Figures S1-S9 and Table S1

Supporting Computational Results: Figures S10, S11

Supporting Experimental Results:

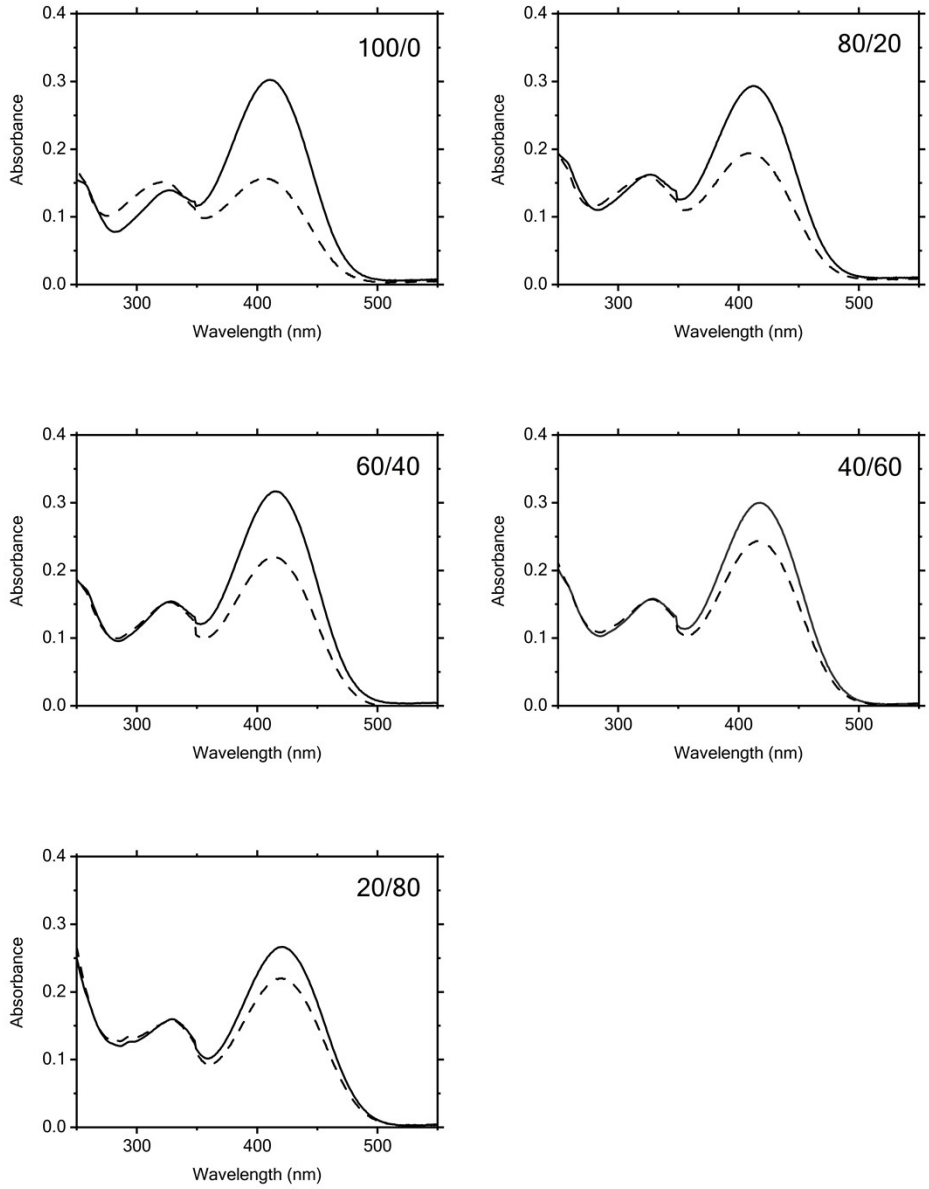

Figure S1. Absorption spectra recorded before (slod line) and after (dash line) time-resolved fluorescence measurements on indazole-mPAH in different water/glycerol (w/w) mixtures as indicated.

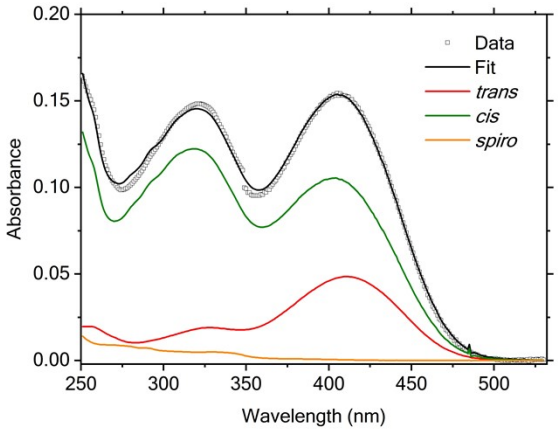

Figure S2. Spectral deconvolution for the absorption spectrum acquired for the ~25 µM mPAH in water after TRF measurement, *i.e.*, the dashed line in the 0 % panel of Figure S1 (symbols), along with its fit (black line), *trans* (red line), *cis* (olive line) and *spiro* (orange line) spectra. The vertical jump at 350 nm in the spectrum depicted by symbols was caused by an instrument error.

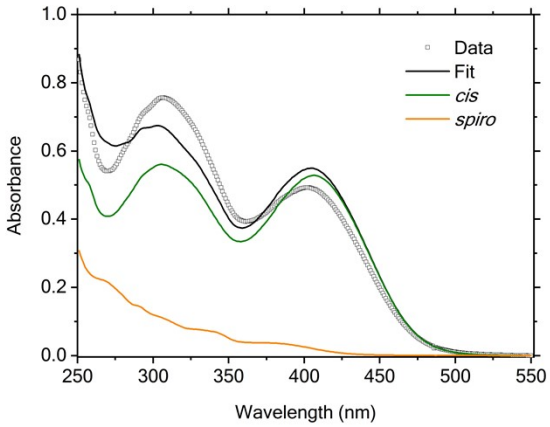

Figure S3. Spectral deconvolution for the absorption spectrum acquired for the 1 mM mPAH in water at a photostationary state under continuous irradiation (Fig. S2, timepoint 3 in Ref. 5 of main text), corresponding to a constant solution pH (symbols), along with its fit (black line), *cis* (olive line) and *spiro* (orange line) spectra; inclusion of the trans spectrum (not shown) does not improve the fit.

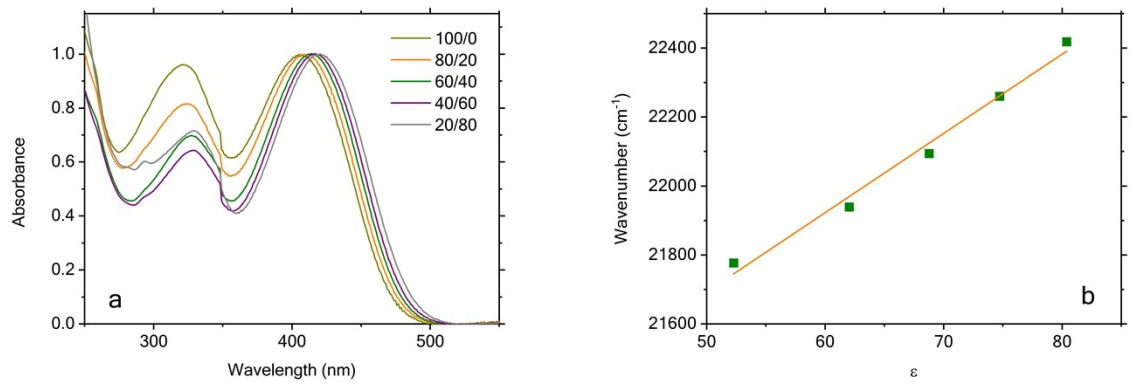

Figure S4. (a) Absorption spectra of indazole-mPAH in different water/glycerol (w/w) mixtures acquired after time-resolved fluorescence measurements. The spectra are normalized to 1.0 at the peak absorption wavelength to ease comparison. (b) The corresponding spectral shift in wavenumber as a function of dielectric constant (symbols) along with a linear fit (line).

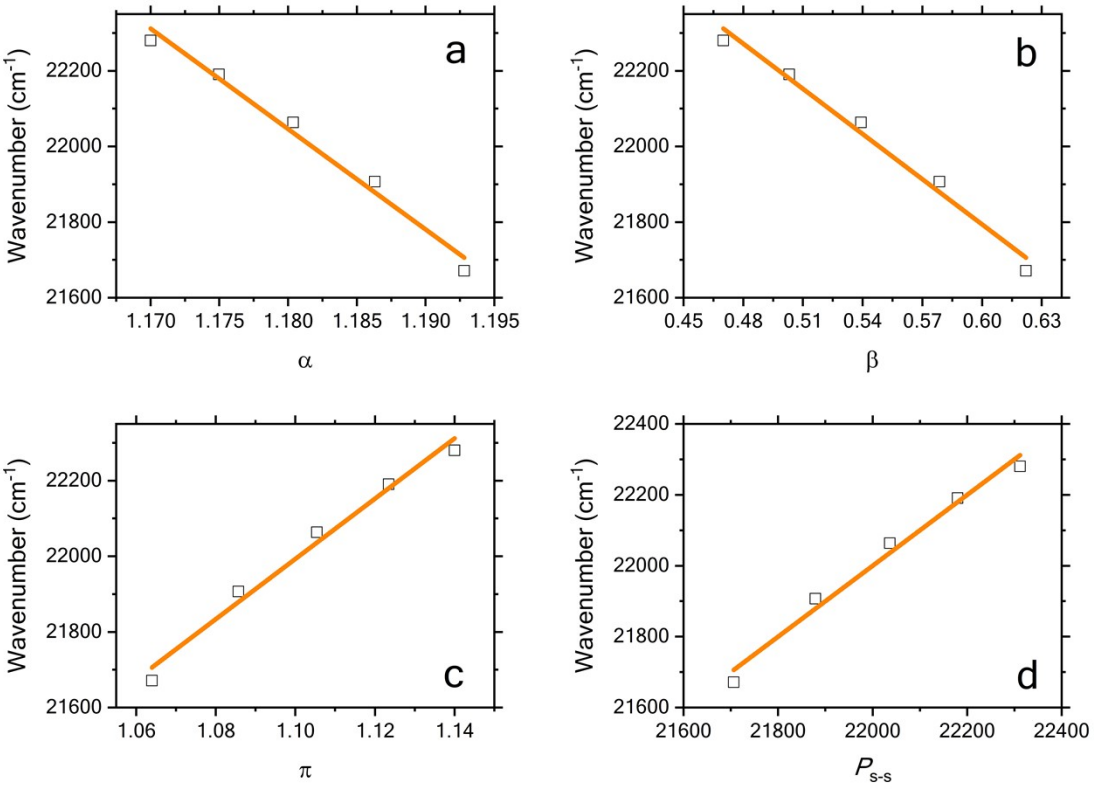

Figure S5. The absorption spectral shift shown in Figure 2B as a function of the Kamlet-Taft parameter α (a), β (b), π^* (c), and their linear combinations P_{s-s} by treating P_{s-s}^0, s, a, and b as fitting parameters (d). The solid lines are linear fits to the data.

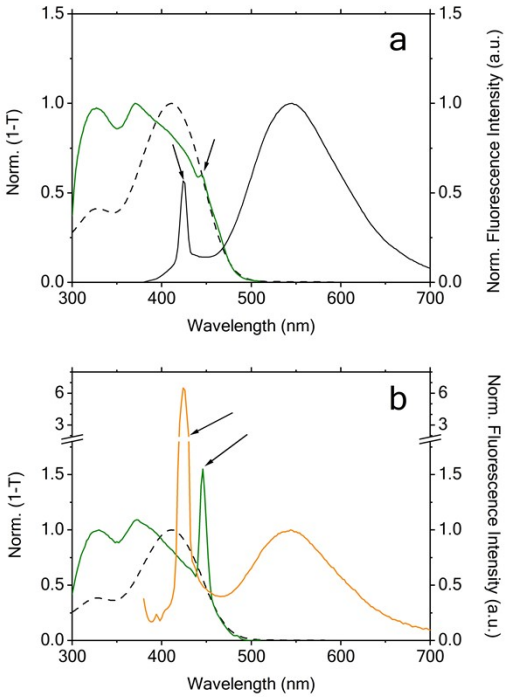

Figure S6. Normalized steady-state fluorescence excitation (olive) and emission (orange) spectra, along with an absorption spectrum (dashed line) plotted as 1-T (transmission) acquired for aqueous solutions of indazole-mPAH with absorbances (transmissions) of (a) 0.112 (77.3 %) and (b) 0.01 (97.7 %) at 411 nm, respectively. The excitation spectrum was recorded by monitoring fluorescence emission at 527 nm, and the emission is collected upon excitation at 370 nm. The arrows indicate the peaks arising from the most intense water Raman feature at 3400 - 3600 cm^{-1}, which are observable in both fluorescence excitation and emission spectra.

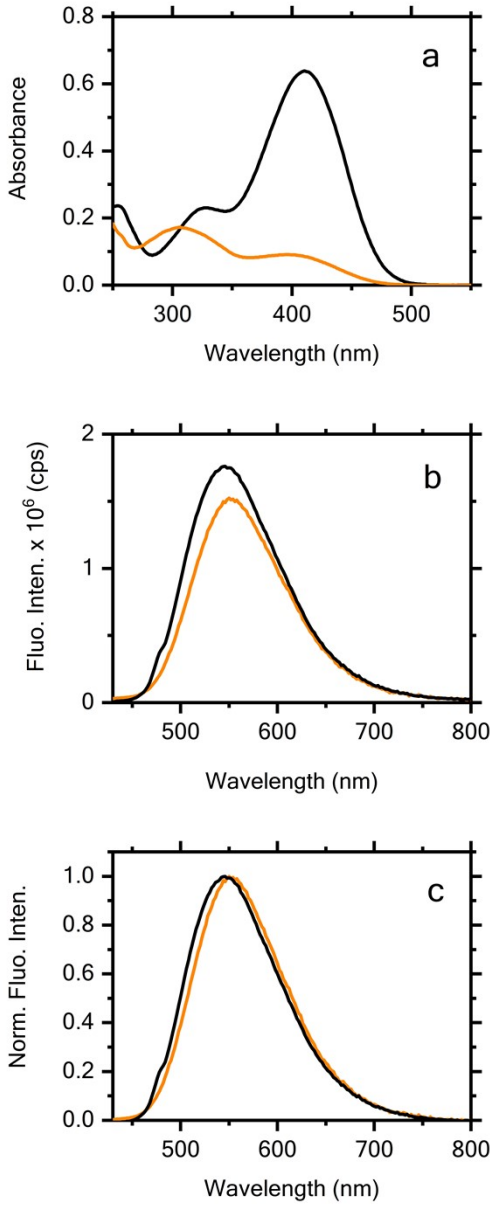

Figure S7. (a) Absorption spectra acquired using a ~25 μM aqueous solution of mPAH before (black line) and after (orange line) irradiation. (b) Corresponding fluorescence emission spectra measured upon excitation at 410 nm (before irradiation) and 315 nm (after irradiation), and further normalized by the sample absorption at these wavelengths. (c) Fluorescence emission spectra normalized to the corresponding maximum emission intensity.

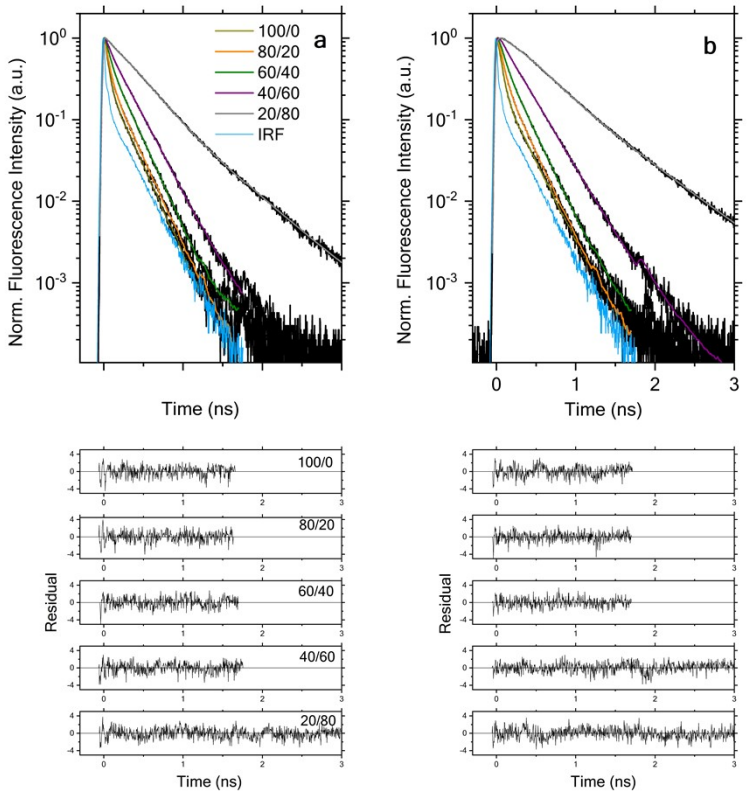

Figure S8. Time-resolved fluorescence data measured at (a) 510 and (b) 550 nm upon excitation with laser pulses centered at 405 nm for indazole-mPAH in different glycerol/water (w/w) mixtures as indicated. The peak intensities are scaled to 1.0 for all data (black lines), the corresponding fits and instrument response function are depicted by color lines. The residuals of these fits are plotted in separate panels labeled by the different glycerol contents.

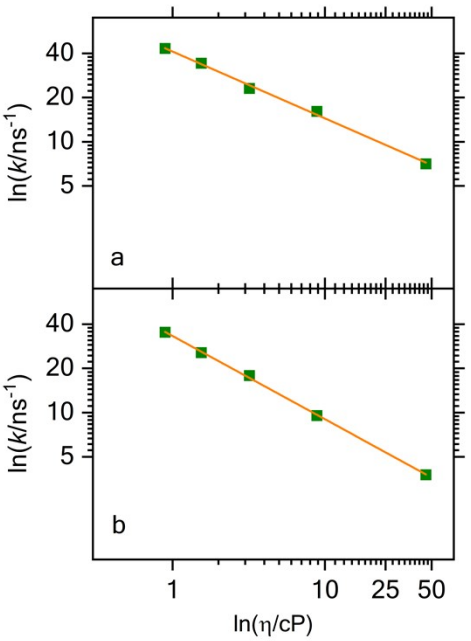

Figure S9. Double logarithmic plots of the average fluorescence decay rates for indazole-mPAH at (a) 510 and (b) 550 nm, respectively, as a function of solution viscosity of different water/glycerol (w/w) mixtures. The solid lines are linear fits to the data.

Table S1. Summary of the lifetimes (τ_1–τ_3) and relative amplitudes (A_1–A_3) extracted for the time-resolved fluorescence decays measured at 510, 530 and 550 nm for various water/glycerol (w/w) mixtures through deconvolution data fitting.

WL (nm)	Water/glycerol (w/w)	τ_1 (ps)	A_1 (%)	τ_2 (ps)	A_2 (%)	τ_3(ps)	A_3 (%)	$\bar{\tau}$ (ps)	χ^2
510	100/0	20.5	92.7	96.8	7.3	193.5	-1.8	23.1	1.390
	80/20	22.0	83.7	91.3	16.3	180.0	-2.8	29.1	1.395
	60/40	23.8	69.8	97.4	30.2	276.7	-1.2	43.2	1.330
	40/60	21.7	60.4	110.6	31.3	171.1	8.4	62.0	1.348
	20/80	28.8	54.7	207.7	36.0	543.1	9.3	140.9	1.145
530	100/0	23.4	90.6	79.0	9.4	180.4	-2.1	25.4	1.776
	80/20	23.8	73.6	77.5	26.2	171.4	-3.2	33.4	1.378
	60/40	28.4	61.0	106.0	39.0	176.7	-5.8	51.3	1.186
	40/60	22.1	43.3	104.5	45.8	221.0	11.0	81.6	1.169
	20/80	40.3	41.1	230.0	42.5	591.1	16.4	211.1	1.159
550	100/0	24.0	79.4	68.0	20.6	114.4	-5.5	28.3	1.435
	80/20	27.7	68.7	79.3	31.3	170.8	-3.7	39.0	1.151
	60/40	27.1	51.7	93.3	48.3	193.7	-2.4	55.8	1.024
	40/60	31.7	36.6	124.9	53.6	264.4	9.8	104.4	1.201
	20/80	45.8	32.4	252.2	46.2	618.5	21.4	263.7	1.218

χ^2: reduced chi-square

$\bar{\tau}$: amplitude weighted average lifetime calculated by $\bar{\tau} = \sum_{i=1}^{3} A_i \tau_i$

Supporting Computational Results

Our theoretical approach was first validated by computing and comparing the absorption spectrum shown in Figure S10 with the experimental spectrum measured in water (Figure 2a). This comparison shows that our TDDFT calculations reproduce all the main features of the experimental spectrum, including the main band in the visible range and a small peak followed by a sharp rise at higher energies, except for the commonly observed systematic energy shift. To analyze orbital contributions to the excited states, we calculated the natural transition orbitals (NTOs) for four lowest transitions, which all show the π character. For example, as illustrated in Figure S10, the S_1 $\pi \rightarrow \pi^*$ transition is dominated (> 97%) by electron excitation from the occupied to unoccupied π C=C bond. Additionally, we have analyzed the change in the dipole moment between the ground-state (S_0) and the first singlet excited-state (S_1) and the corresponding difference in the electron density. A decreased dipole moment in the S_1 state is found to result from a change

in the electron density (see Fig. S11) that is mostly localized around and next to the C=C bond with an increasing electron density (red color) in the electron-rich benzothiazolium ring and a decreasing electron density (blue color) in the electron-rich indazole ring. The results are described in the main text, which are fully consistent with the pronounced negative solvatochromism observed in the absorption spectra (Figure 2a,b).

To compute a fluorescence spectrum, geometry optimization for excited states is required. Starting from the Franck-Condon geometry for the planar *trans* isomer of the model indazole-mPAH (see Computational Methods above), our geometry optimization results in a S_1 minimum structure that maintains the planarity. The computed vertical $S_1 \rightarrow S_0$ transition at 527 nm is also very close to the peak wavelength of the fluorescence spectra (~530 nm) acquired experimentally. However, our calculations predict that the *cis* isomer is not a stable minimum on the S_1 surface, as it undergoes a barrierless rotation around the C=C bond and adopts a twisted geometry with a dihedral angle close to 90^o during the geometry optimization. The potential energy scan for the rotation around the double bond in the S_1 state further confirm a very different landscape of the PES for the *trans* and *cis* forms (Figure 5). Our calculations further predict zero oscillation strength for $S_1 \rightarrow S_0$ transition at the twisted S_1 global minimum geometry. We also performed a transition state search to identify the structure connecting the *trans* and the twisted geometry on the S_1 PES to provide a more accurate estimate of the reaction barrier. We found that the C-C=C-C dihedral angle did not closely follow the H-C=C-H dihedral angle in the region very close to the transition state. We therefore independently varied these two degrees of freedom to accurately map the reaction coordinate and locate a transition state with the C-C=C-C and H-C=C-H torsional angles of 122^o and 113^o, respectively. The inclusion of the vibrational contributions to the electronic energies reduced the reaction barrier from 3.8 to 2.6 kcal/mol.

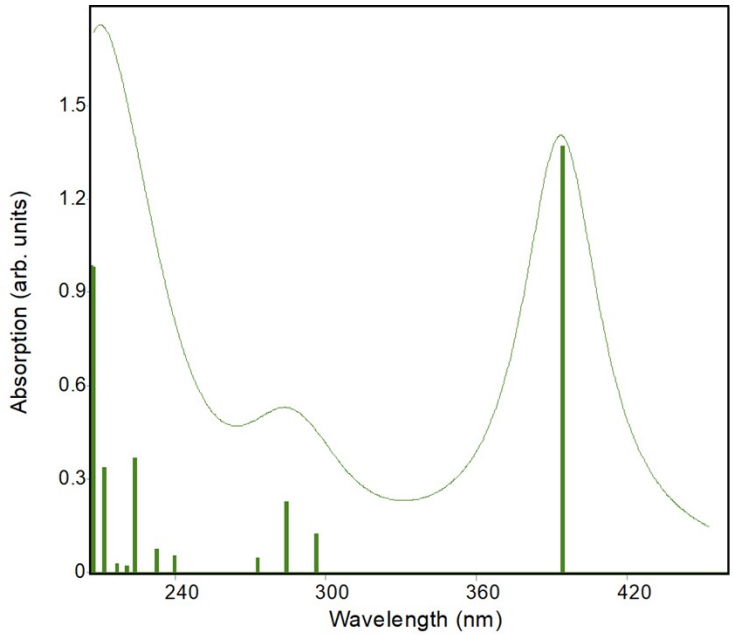

Figure S10. The simulated absorption spectrum for the model indazole-mPAH obtained using the TDDFT method for vertical excitations (stick lines). The solid line represents a homogeneously broadened spectrum described by a Lorentzian function.

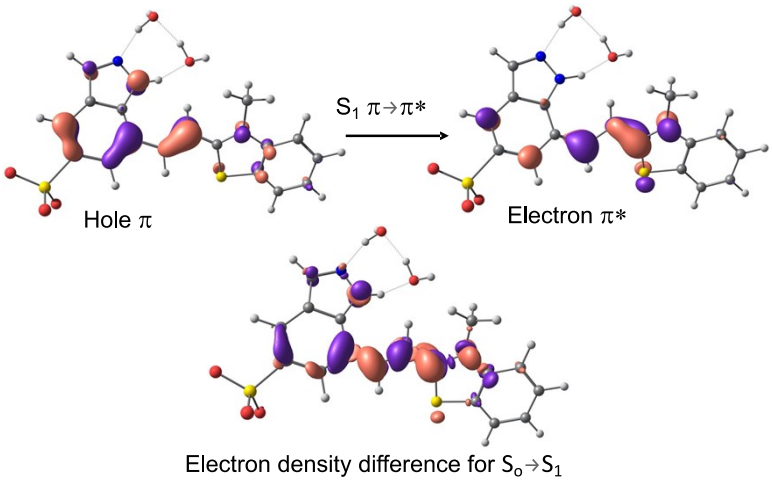

Figure S11. Frontier natural transition orbitals (NTOs) and the electron density difference plots for the S_1 $\pi \rightarrow \pi^*$ transition.